





Scaled seismotectonic models of megathrust seismic cycles through the lens of dynamical systems theory

F. Corbi *, A. Gualandi ^{2,3}, G. Mastella ⁴, F. Funicello ⁵

¹Istituto di Geologia Ambientale e Geoingegneria - CNR c/o Dipartimento di Scienze della Terra, Sapienza Università di Roma, Rome, Italy, ²Bullard Laboratories, Department of Earth Science, University of Cambridge, UK, ³Osservatorio Nazionale Terremoti, Istituto Nazionale di Geofisica e Vulcanologia, Rome, Italy, ⁴Sapienza University of Rome, Earth Sciences, Rome, Italy, ⁵Dipartimento di Scienze, Laboratory of Experimental Tectonics, Università “Roma TRE”, Rome, Italy

Author contributions: *Conceptualization:* FC, AG. *Data curation:* FC, GM,. *Formal analysis:* FC, AG. *Funding acquisition:* FF. *Investigation:* FC, GM, AG, FF. *Methodology:* FC, AG. *Resources:* FC, FF. *Validation:* FC, AG. *Visualization:* FC. *Writing – original draft:* FC. *Writing – review & editing:* FC, GM, AG, FF.

Abstract We investigate the physics of laboratory earthquakes in scaled seismotectonic models of megathrust seismic cycles. We study models of different sizes, materials, deformation rates, and frictional configurations. We use nonlinear time-series analysis tools to characterize the dynamics of the experiments. Observations are described, on average, by a low-dimension (<5), similar to slow slip episodes in nature and friction experiments performed with quartz powder. Results seem insensitive to the along-strike frictional segmentation of the megathrust. Using displacement as an input variable, the instantaneous dimension and the instantaneous extremal index vary through the seismic cycles. We notice the highest values of the instantaneous dimension associated with slip phases. Under specific circumstances, clear drops of the instantaneous extremal index can serve as an early indicator of slip episodes. Prediction horizons in the order of slip duration mirror similar predictability as for slow slip episodes in nature. We conclude that seismotectonic models are effective tools to study frictional physics despite their different spatio-temporal scales.

Non-technical summary Are scaled seismotectonic experiments just toy models, or do they share the same physics as natural prototypes? In this paper, we computed relevant parameters to characterize system dynamics and we found that laboratory experiments are characterized by remarkably similar complexity to those observed for slow slip events from the Cascadia and Hikurangi subduction zones. We use dynamical systems theory to constrain how much information is needed to describe the evolution of the experiments over time and their predictability. These observations highlight that scaled seismotectonic experiments can be useful for investigating earthquake dynamics due to common frictional physics across different spatio-temporal scales.

Production Editor:
Carmine Galasso
Handling Editor:
Pathikrit Bhattacharya
Copy & Layout Editor:
Théa Ragon

Signed reviewer(s):
Martijn van den Ende

Received:
March 26, 2024
Accepted:
January 20, 2025
Published:
February 25, 2025

1 Introduction

Detailing the spatio-temporal evolution of the seismic cycle of subduction megathrusts is fundamental for seismic hazard assessment. Precise surface displacement measurements allow for identifying locked and creeping megathrust segments, which might provide first-order insights into future rupture scenarios (e.g., Moreno et al., 2010; Avouac, 2015). However, despite recent efforts to increase the spatial density of geodetic networks, scientists face the problem of having access only to a fraction of the seismic cycle: the instrumental record of a few tens of years is way shorter than the multi-century return period of large earthquakes.

A valid alternative for studying the seismic cycle of subduction megathrusts is via analog and numerical modeling. Both analog and numerical models are beneficial for understanding how a given physical property influences seismicity characteristics over multiple seismic cycles (e.g., Brizzi et al., 2020; Corbi et al., 2017). Analog models have been used for over a century to in-

vestigate several geologic and seismotectonic processes (e.g., Rosenau et al., 2019; Funicello and Corbi, 2021). Differently from other laboratory earthquake experiments, such as dynamic rupture experiments (e.g., Xia et al., 2004) or rock friction experiments (e.g., Scuderi et al., 2016), seismotectonic analog models are built following the similarity criteria: the size of the model, implemented materials, and deformation rates are set considering geometric, kinematic, dynamic, and rheological scaling factors (Hubbert, 1937). Hence, a seismotectonic analog model represents a small-scale reproduction of a “seismogenic” subduction zone (in our case) where stresses and velocities are proportionally smaller/slower than in real Earth. An additional key feature of analog models is the introduction of a time scaling factor that allows mimicking hundreds of seismic cycles in a few minutes, overcoming the observational bias due to incomplete records in nature. A potential drawback of seismotectonic analog models is their simplistic nature. Among the various simplifications, the majority of scaled seismotectonic models feature homogeneous upper plate rheology, undeformable

*Corresponding author: fabio.corbi@igag.cnr.it

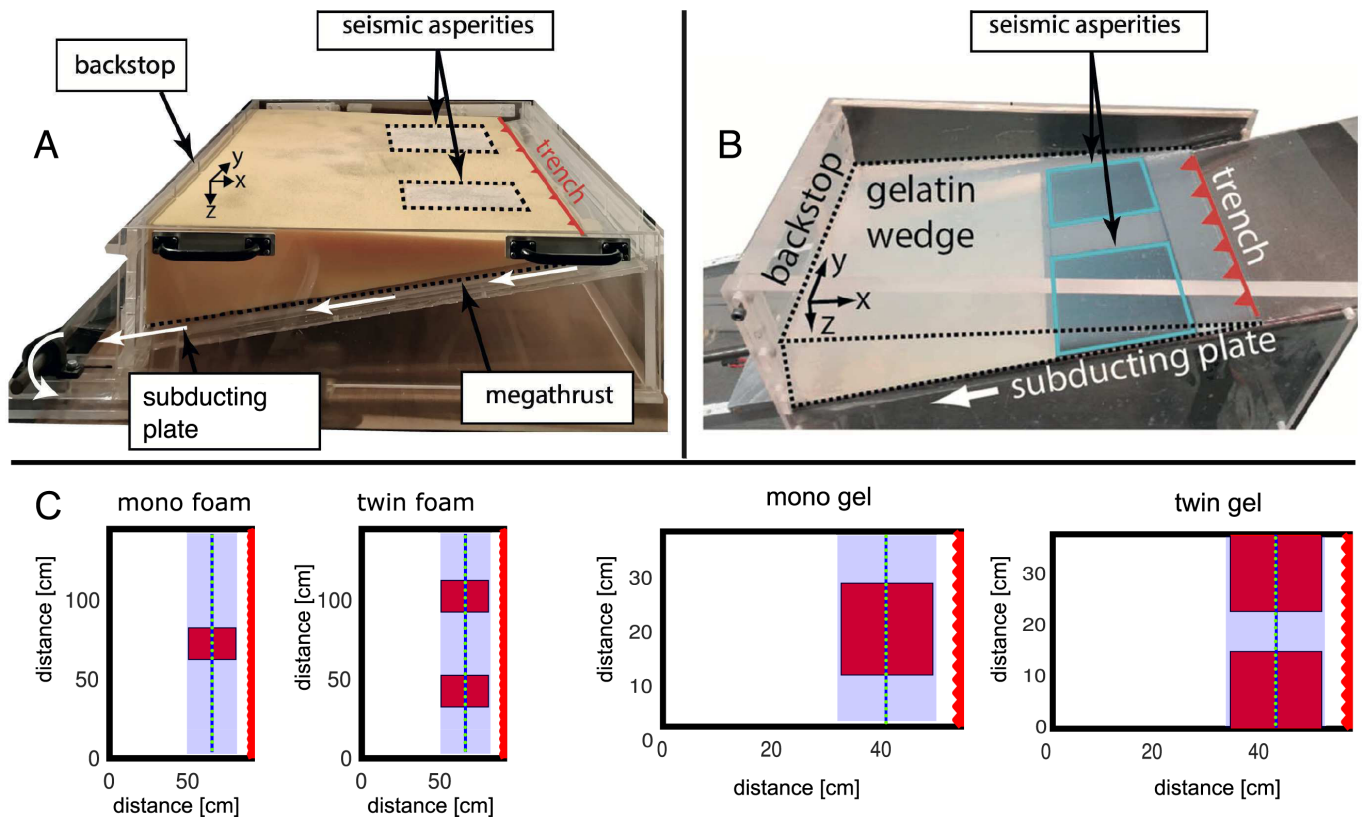


Figure 1 Oblique view photographs of experimental setups (Foamquake and Gelquake represented in panel a and b, respectively; modified from Mastella et al., 2022b) Both photos display twin asperities configurations. Panel c shows sketches of the four analyzed experiments with red areas representing asperities. Blue lines and blue shaded areas represent the analyzed cross-section and the seismogenic area, respectively. Cross sections are discretized in 28 and 29 target points (highlighted by green points) in Gelquake and Foamquake, respectively.

slab, constant loading, the lack of a scaled temperature and phase transitions, and the absence of mantle/lithosphere coupling (e.g., Rosenau et al., 2019).

Determining if seismotectonic analog models share the same underlying physics as the natural prototype is crucial to verify their effectiveness as investigation tools. To address this question, we rely on dynamical system theory (e.g., Strogatz, 2024) and explore the behavior of analog models with different rheology and frictional configurations of the analog megathrust. We focus on two metrics: the system dimension and the predictability horizon of laboratory earthquakes. The system dimension is a useful measure of complexity, being informative of the number of degrees of freedom (*dof*) needed to explain a dynamical system (Theiler, 1990). Predictability is another useful quantity to describe how much information we gain with the evolution of the system (Eckmann and Ruelle, 1985; Boffetta et al., 2002).

We discuss analogies and differences of computed parameters between different models, to highlight their relevance for seismic cycle dynamics. The study compares the findings against the dynamics of slow earthquakes (Gualandi et al., 2020; Truttmann et al., 2024) and laboratory earthquakes produced in double-direct shear experiments (Gualandi et al., 2023). Scaled seismotectonic models are found to have remarkably similar system dimensions and predictability as slow slip episodes (SSEs) that occur in the Cascadia and Hiku-

rangi subduction zones, as well as friction experiments performed with quartz powder. This result shows the usefulness of seismotectonic models as robust investigation tools to shed light on the behavior of megathrust seismic cycles.

2 Data

Data used in this study comprises surface deformation time-series generated by two scaled seismotectonic models: Foamquake and Gelquake (Figure 1). The names of the models reflect the overriding plate materials (Corbi et al., 2013; Mastella et al., 2022a). Both models feature a wedge-shaped overriding plate underthrust by a 10° dipping, flat plate, mimicking the subduction environment. Model dimensions allow reproduction of a scaled-to-nature subduction segment of 330x220 km² and 310x510 km² in the trench orthogonal and parallel directions for Gelquake and Foamquake, respectively (Supplementary Information -SI- Table S1). In both models, subduction is driven with a stepping motor at a rate of 0.01 cm/s. Monitoring is performed from the top view with a video camera, acquiring images at 7.5 and 50 frames per second for Gelquake and Foamquake, respectively. Such framerate is high enough to illuminate slip phases with few unit- few dozen frames, similar to daily GNSS monitoring of slow slip events in nature. After an initial stress build-up period, models experience stick-slip dynamics, which

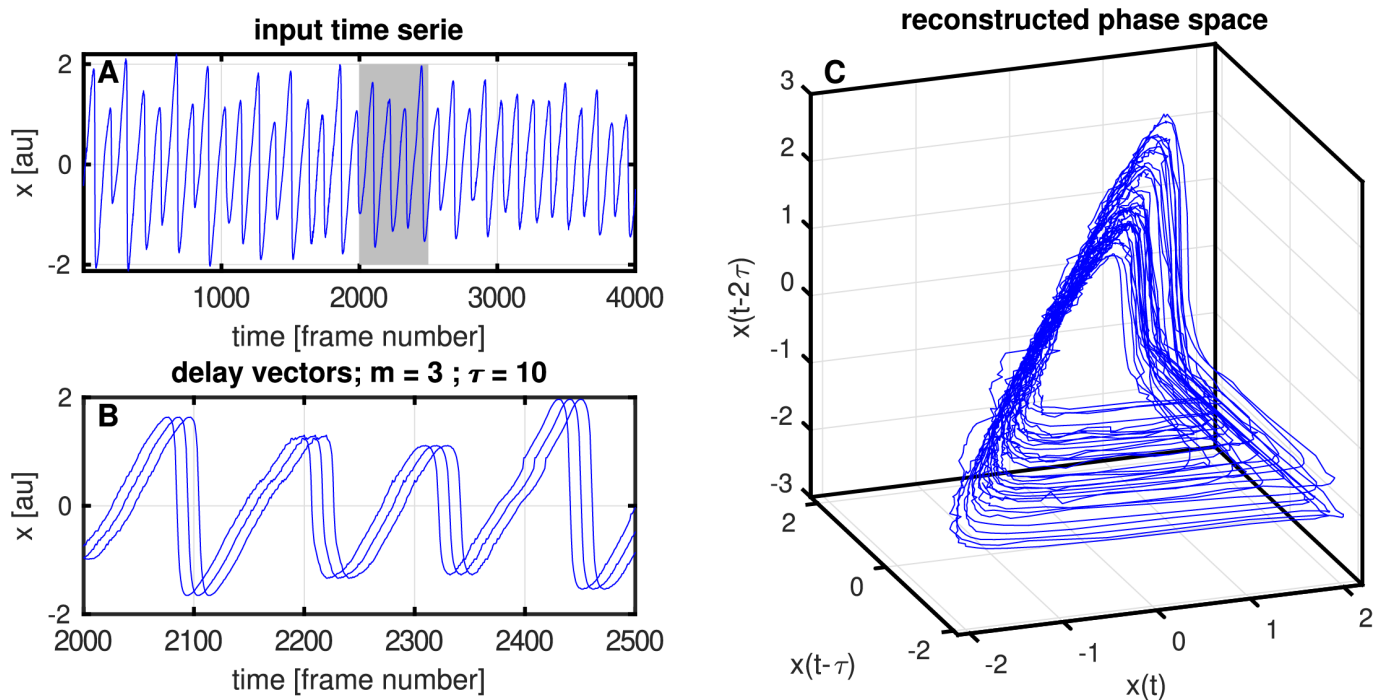


Figure 2 Typical time series $x(t)$ from a target point located at the center of the asperity from the mono gel experiment (panel A). The graph shows a typical stick-slip behavior as manifested in our experiments. The gray rectangle in the background highlights a fraction of the time series reported in panel B as delay vectors where, to give an example, $m=3$ and $\tau=10$ are used. Reconstructed attractor in the time delay phase space (panel C).

is captured by Particle Image Velocimetry (PIV; Sveen, 2004) as long phases of slow, landward motion (i.e., stick phases) alternating with trenchward motion (i.e., slip phases). By integrating horizontal (x-y plane) velocity time series from PIV (knowing the time between consecutive frames), we obtain displacement time series describing model surface deformation (e.g., Figure 2A), similar to a dense homogeneously distributed geodetic network (Corbi et al., 2019). PIV illuminates a variable number of seismic cycles between 34 and 67 in each model run.

To investigate how the frictional segmentation of the megathrust affects the analog seismic cycle dynamics, we conduct mono- and twin-asperity (i.e., stick-slipping areas) experiments for each overriding plate material, totaling four experiments: mono-gel, twin-gel, mono-foam, and twin-foam. Asperities have downdip extent and depth range scaling with the corresponding parameters computed as the global average of subduction megathrust seismogenic zones (Heuret et al., 2011). One relevant difference between Gelquake and Foamquake is the nature of the plate interface: the former is a bimaterial contact and the latter is created by a 1 cm thick granular layer mimicking the subduction channel. Asperities are reproduced with a gel-on-sandpaper interface and with a rice layer in Gelquake and Foamquake, respectively, both ensuring stick-slip dynamics. Depending on the experiment's configuration, asperities are surrounded or separated by a gel-on-plastic interface in Gelquake and by a layer of quartz sand in Foamquake.

For each experiment, we analyze displacement time series sampled along a cross-section striking parallel to the trench and located at the downdip center of the as-

perity and from the whole seismogenic area (Figure 1). Pre-processing is performed for data standardization across different experiments (SI Text S1).

3 Methods

We treat scaled seismotectonic models as dynamic systems and aim to determine their dimension (D). We compute D with two different methods: one based on Embedding Theory (ET, Takens, 1981; Sauer et al., 1991) and the other on Extreme Value Theory (EVT, Faranda et al., 2017). The two approaches are based on different assumptions.

The method of time delay embedding allows estimating D from the knowledge of the time evolution of a single system variable. In our case, this is very useful because we have access only to the displacement and velocity time series, but other variables might participate in the dynamical evolution of the system (e.g., in the rate- and state-framework to describe friction, a state variable is used to allow for healing of the fault, Dieterich, 1979; Rice and Ruina, 1983). Time delay embedding involves duplicating the original time-series m times with a τ time-step shift between each copy (i.e., delay vectors; Figure 1b). m refers to the minimum embedding dimension while τ refers to the time delay. Then, the reconstructed phase space can be visualized by plotting the values of delay vectors. We use classical approaches based on information theory to estimate τ (Fraser and Swinney, 1986), and on false nearest-neighbors to estimate m (Cao, 1997).

The method based on EVT uses the Poincaré recurrence theorem and exploits the density of nearest neigh-

bor configurations to estimate the instantaneous dimension of the system. Contrary to ET, we do not take an embedding of the observed time series but consider a configuration ζ as a particular recorded frame. Looking at how distant are similar frames during an experiment, we can estimate the density of neighbors and the dimension of the system (Faranda et al., 2017). The two main advantages of this approach are: i) there is only one parameter to set, i.e., the radius of the ball defining the neighbors or the number of nearest neighbors to use, and this can be stated via a quantile threshold q on the distances; ii) we retrieve instantaneous values of the dimension $d1$, and (under ergodic assumption) the time average gives us the average dimension of the system.

The following two remarks are important to interpret our results:

- 1) Taken's theorem (1981) provides the condition for preserving the topological features of an original trajectory. The theorem states that the embedding dimension m must be at least larger than twice the true dimension D (i.e., $m \geq 2D+1$) of the underlying system (e.g., Huke, 2006). If the functions governing the dynamics are sufficiently smooth, certain properties can be preserved with values of m smaller than $2D$, except for subsets of dimension size no greater than $2D - m - 1$ (Sauer et al., 1991). Cao's method (1997) allows us to determine the minimum embedding dimension, which cannot be smaller than D (i.e., $D \leq m$). Thus, once m is determined, we can set bounds on the true dimension of the system, D , as $(m-1)/2 \leq D \leq m$.
- 2) There are many ways to calculate the dimension D of a dynamical system from observed time series (Theiler, 1990). Despite some discrepancies, all should agree in telling us what is the number of *dofs* needed to characterize the attractor. For this reason, we will not make differences between the various dimensions, but just refer to the estimated values with the letter D .

Another quantity that we can estimate with the EVT is the instantaneous extremal index θ . This is the inverse of the persistence, normalized between 0 and 1. It gives us information about the predictability of the system. In fact, the persistence indicates for how long the dynamics stay close to a certain configuration. If the persistence is very large/small, knowing that we are in a similar configuration tells us that we have high/low chances to get a similar configuration at the next time step. A connection between the Dynamical Extremal Index (DEI) Θ and the metric entropy H (i.e., the sum of all positive Lyapunov exponents) has been established by Faranda and Vaienti (2018). While for the dimension index we could average D over time to get D , we cannot simply average θ over time to get Θ . Nonetheless, we can expect Θ to belong to the range $(\theta_{\min}, \theta_{\max})$. We can thus estimate a range of possible values for H (e.g., Gualandi et al., 2020). This quantity is equal to the sum of all positive Lyapunov exponents, and we use its

inverse to define a predictability horizon t^* . An alternative way to evaluate H , based on ET and rooted in information theory, is via Nonlinear Forecasting Analysis (NFA, Farmer and Sidorowich, 1987; Wales, 1991). In practice, we split the data into train and test sets. Then, we find the nearest neighbors to a point in the embedded space and we use them to calculate the best linear approximator to map the evolution of the system to T_p time steps into the future. The forecast correctness on the test set is expected to decrease with increasing forecasting horizon. The quality of the forecast can be assessed either via the root mean squared error (ϵ) or via the correlation coefficient (ρ) between observed and forecasted values. The metric entropy is the average rate of information creation, and it measures how quickly the forecast becomes bad. More details on the two techniques and on the choice of the parameters is provided in the Supplementary Information.

4 Results

We define the trench orthogonal component of displacement (x) as the main variable describing the dynamics of our experiment (SI Text S1). The time series of x illustrates the stick-slip behavior, resembling that of shear stress in rock friction laboratory experiments or the slip potency deficit of natural slow slip events (Figure S1-S4).

The analysis of displacement time series from a cross-section striking parallel to the trench shows a minimum embedding dimension m ranging from 3 to 9 for mono asperity experiments and a slightly narrower range (i.e., 3 to 6) for twin asperity experiments (Figure 3A, B, D, E). Distributions of m appear rather constant along the strike of the experiments, except for mono gel where higher m values are observed in concomitance with the asperity. Within individual experiments, the mode of m is 4-5 (Figure 3C, F) which provides a first indication of D in the 2-5 range. This observation suggests that Gelquake and Foamquake dynamics can be represented in a space with a similar number of dimensions (on average), despite significantly different visual appearances displacement timeseries.

Next, we use the EVT to track changes in system dimensions through experimental time. We focus on the asperity area of mono gel to illustrate the result and report similarities and differences with other experiments. Figure 4A, B show that $d1$ and θ display cyclical temporal variations. $d1$ and θ are correlated (Figure 4C), meaning that when the dimension is high, the system is visiting a region of the phase space with transient characteristics. We want to understand how $d1$ and θ vary during individual seismic cycles. To emphasize this pattern, we conduct a k-means analysis to split the data into 4 clusters based on their distribution in the $d1, \theta, x$ space (Figure 4D, S5). The early interseismic (or postseismic) stages are characterized by low $d1$ and θ values. During the interseismic- and late interseismic stages, the values of $d1$ are comparable to each other but higher than early interseismic. Additionally, θ increases during the interseismic and then decreases in the late interseismic stage. This seems reasonable, since the in-

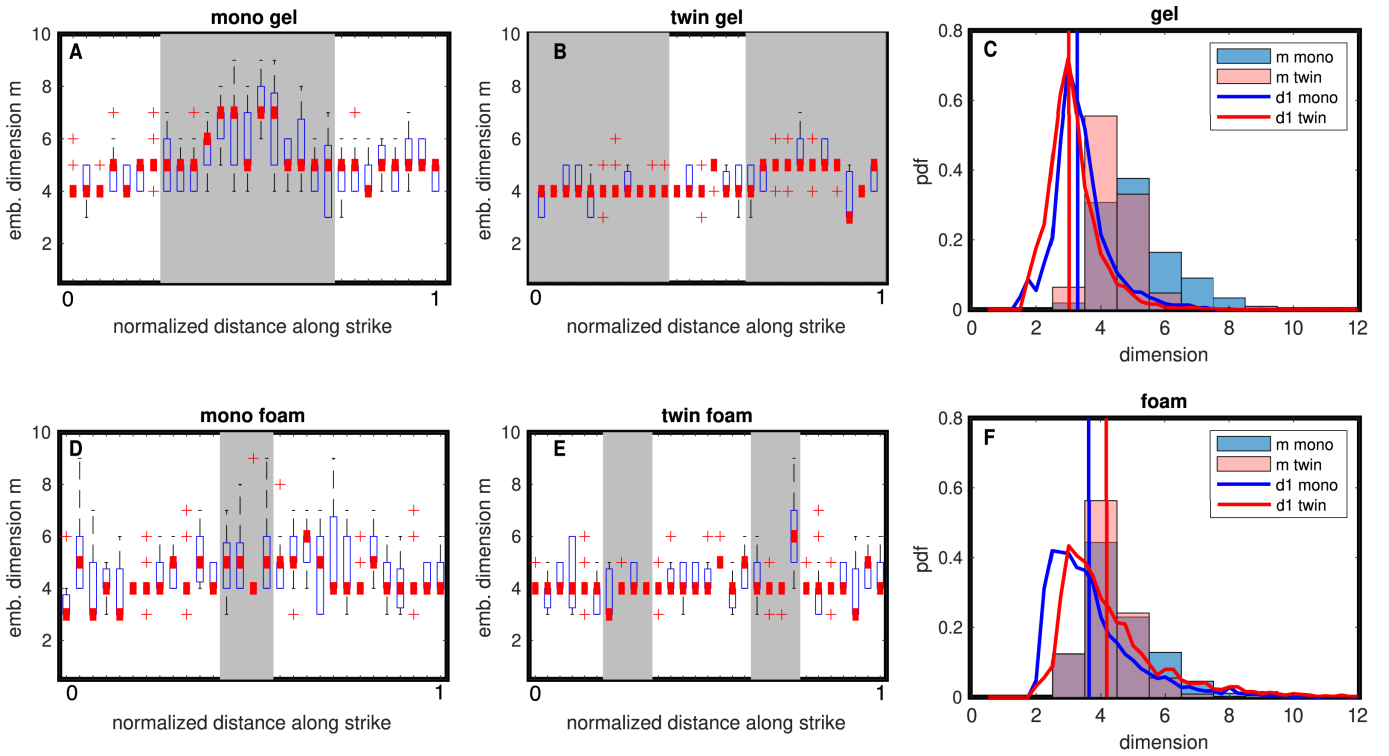


Figure 3 Along strike variation of the embedding dimension m (panels A, B, D, E). The boxplots represent the distribution of m for a specific $x(t)$ along the sampled section. The red squares and open blue rectangles represent the median. The bottom and top edges of open blue rectangles indicate the 25th and 75th percentiles, while whiskers extend to the most extreme data points. Outliers (i.e., a value that is more than 1.5 times the interquartile range away from the bottom or top of the box) are represented by the red + symbols. Gray shaded areas represent the location of the asperities. Panels C and F report the distribution of dimensions for mono and twin asperity configuration experiments in ensemble (i.e., obtained by considering the 15 retrieved m for all target points of the section), respectively. The results relative to the ET and EVT are represented with bars and lines, respectively. The vertical lines represent the mean of $d1$ distributions for different experiments.

put time series shows yielding and a plateau when approaching the rupture, suggesting that here the configurations should look similar to those temporally adjacent. Coseismic stages are characterized by markedly higher $d1$ than previous stages, while θ values return to high values, similar to those of the interseismic stage. When analyzing the two asperities of the twin gel experiment, we notice a similar pattern with low values of θ at x extremes. However, this pattern disappears after selecting the entire seismogenic area (Figure S6). The seismic cycle in the $d1$, θ , x space is less clear when using Foamquake (both mono and twin experiments; Figure S7) although all experiments indicate higher $d1$ during coseismic stages (Figure S8).

By averaging $d1$ over all possible configurations ζ , i.e., averaging $d1$ over time, the EVT shows $D=3.3-3.0$ for Gelquakes (mono and twin, respectively) and $D=3.6-4.2$ for Foamquakes (mono and twin, respectively). Interestingly, the distributions of $d1$ for the four experiments appear to be similar according to model type (gel or foam) rather than by frictional configuration (mono or twin asperity, Figure 3C,F; Figure S9).

NFA shows better prediction performances for Gelquake compared to Foamquake. Independently from the prediction time and target point, ρ is systematically larger in Gelquake than in Foamquake, and the opposite applies to Θ (Figure 5A, B). Predictions accuracy is higher within the asperity compared to

neighboring segments for mono asperity experiments (Figure 5C and E).

The ranges of t_{EVT}^* are similar among the four experiments and are marked by lower and upper values of $\sim 2-5$ frames and $\sim 16-27$ frames, respectively, in relation to the coseismic and interseismic stages (Figure 5C-F). $t_{\rho}^* \sim 2-5$ is about constant in all the four experiments and matches the lower limit of t_{EVT}^* , except for twin gel. In mono gel $t_{\rho}^* > 5$ frames occurs at the asperity periphery and neighboring segments, though the quality of predictions is lower, as indicated by the large error bars (Figure 5C). t_{Θ}^* is systematically larger than t_{ρ}^* in Gelquake (i.e., 5-17 frames) and it cannot be estimated in Foamquake due to inaccurate predictions. Twin gel shows a clear variation of predictability horizons depending on frictional properties as depicted by the lower t_{Θ}^* between the two asperities (Figure 5D).

5 Discussion and Conclusions

5.1 Gelquake vs Foamquake

Both the experimental settings Gelquake and Foamquake are complex systems, with potentially many interacting parts. This is highlighted by the maximum instantaneous dimension that reaches values of a few tens for the various experiments (with the first integer above $\max(d1)$ ranging from 9 to 26 for the different

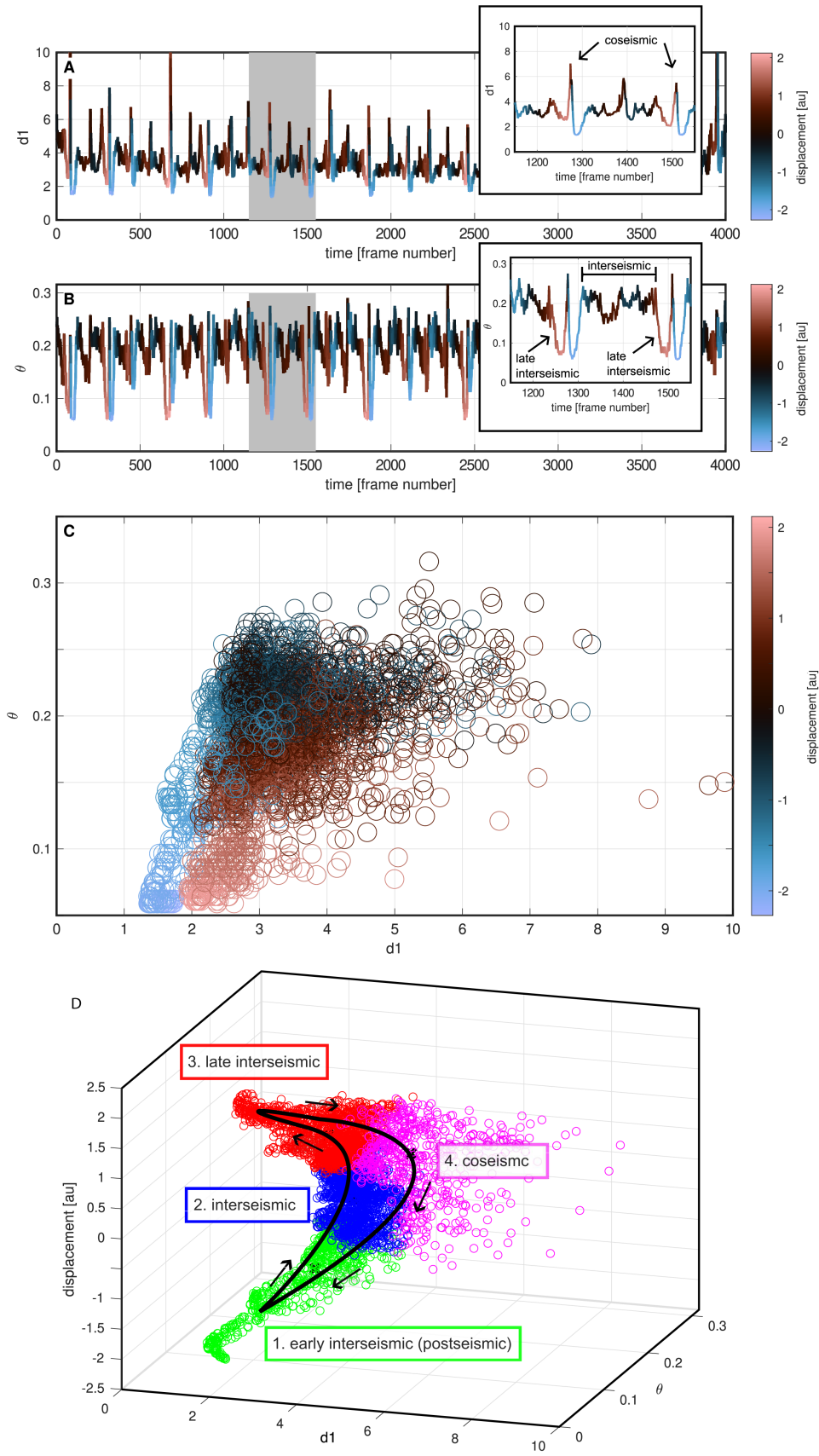


Figure 4 Temporal evolution of $d1$ and θ from the asperity area of experiment mono gel (panels A and B, respectively). The time series are colorcoded by displacement (light blue and pink colors represent early- and late-interseismic stages, respectively). The gray rectangles in the background highlight a fraction of the time series that is zoomed in the insets. A clear decrease of θ characterizes the late interseismic stage. Bivariate plot of $d1$ against θ colorcoded by displacement reveals a peculiar arrangement of different stages of the analog seismic cycle in the $d1$ - θ plane (panel C). Panel D shows the analog seismic cycle path in the $d1$, θ , displacement space, with marker colors representing different stages as identified by k-means analysis to split data into 4 clusters given their distribution. To zoom into the region of interest, in panels C and D we set a boundary at 10 units on the $d1$ -axis, even though few data points extend up to 25 units.

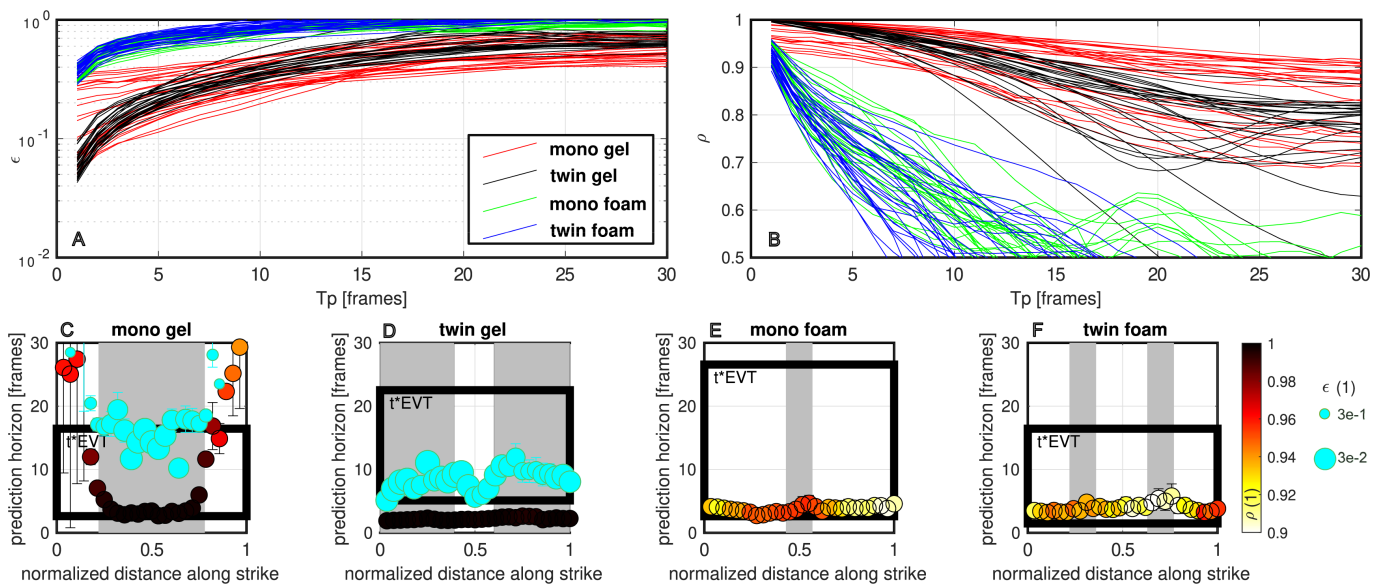


Figure 5 NFA performances and prediction horizons. Prediction performances as a function of prediction time T_p as quantified by Θ and ρ (panels A and B). Large values of Θ and small values of ρ indicate a poor performance of the forecast. Lines refer to different target points along the sampled section parallel to the trench. Prediction horizons for different experiments (panels C-F). Black boxes represent the range of t_{EVT}^* . Circles refer to t_{ρ}^* , with colorcoding highlighting the quality of predictions at $T_p = 1$. Cyan circles represent t_{Θ}^* , with the size of circles proportional to $1/\Theta$ at $T_p = 1$. Errorbars for t^* are proportional to the standard deviation of the linear fit computed to estimate H (SI text 4). Gray shaded areas represent the location of the asperities.

experiments). Nonetheless, our analysis supports the existence, on average, of a low dimensional (<5) attractor describing the dynamics of scaled seismotectonic models, suggesting that a reduced-order model may be suitable to explain the macroscopic observations. Foamquake is more complex than Gelquake as indicated by their higher average D and lower prediction performances. The origin of the higher complexity of Foamquake may derive from the granular layer analog of the subduction channel. Although both Gelquake and Foamquake can be classified as elasto-plastic models for the applied strain rates (Van Der Pluijm and Marshak, 2004), stress heterogeneities developing over multiple stick-slip cycles within the Foamquake’s granular layer may account for the additional degree of freedom compared to the simple bimaterial frictional interaction of Gelquake. To a first approximation, we can consider the granular layer on Foamquake as the analog of a fault gouge in nature where complexity emerges from inter-grain interactions (e.g., grains rotation, force chains development) and interaction between the granular layer and the overriding plate. Our results suggest the possible need for an extra *dof* to explain the complexity of elasto-plastic models when coupled with a granular shear zone. Given the relatively faster nature of Foamquakes, the extra *dof* may be related to dynamic effects that become important. If that is the case, and extrapolating to nature, we could expect a higher number of *dofs* to characterize earthquakes with respect to the ones needed for slow earthquakes.

5.2 Similarities and differences with slow slip episodes and double direct shear labquakes

Our analysis shows that scaled seismotectonic models have similar system dimensions as SSEs in nature. Specifically, Gelquake, has a dimension of $D=3.0-3.3$, which is remarkably similar to the $D=3.1-3.5$ of SSEs observed in the Cascadia subduction zone (Gualandi et al., 2020), one of the areas with the longest geodetic record of SSEs (Michel et al., 2018). SSEs from the Hikurangi Subduction Zone appear more irregular in terms of recurrence than those from Cascadia (likely due to interacting sources at different depths along the plate interface). Despite this, a recent study found a low-dimension, at least for the shallow SSEs where the signal contains less noise (Truttmann et al., 2024).

Similar low system dimensions (<5) have been recently deduced analyzing laboratory earthquakes from a double direct shear apparatus, capable of producing both fast, slow, and alternating fast and slow slip episodes (Gualandi et al., 2023). These observations support a unifying view where slip episodes in the laboratory and SSEs in nature share similar complexity (i.e., *dof*) despite the different scales.

It is worth noting that the retrieved average dimension is surprisingly small, and this could be the result of a bias induced by the limited number of available data. A recent review pointed out that it might be difficult to directly relate the calculated dimension with the actual number of *dofs* of the system (Datseris et al., 2023). In fact, we are not estimating the true number of *dofs*, but just the effective number of *dofs* accessible via the observations. Both lab- and nature-scale phenomena are highly complex, with possibly many true

dofs. A recent study looked at numerical simulations of the SSEs cycle, where the true number of *dofs* was large and known (several thousands, Gualandi et al., 2024). The estimated average dimension in that case was still low (<5), but spikes of instantaneous dimension of a few thousands indicated that the complexity could not be captured just by the average quantity. A similar point can be made here: despite the ambiguity in the actual number of *dofs*, we can still argue that higher values of dimension indicate higher complexity of the system, and the variation through the seismic cycle of this complexity can help us understand in which phase of the cycle the system is. Understanding whether same conclusions hold also for regular earthquakes deserves future investigations.

Another common point of scaled analog models with SSEs is predictability. Here we found that slip episodes have prediction horizons in the 2 - 5 frames range i.e., a horizon comparable with a fraction of slip durations. This observation seems to support the idea that it is difficult to forecast the final rupture size based on the characteristics of the rupture onset (Meier et al., 2017) as opposed to a deterministic view where the size of an earthquake is distinguishable early in its rupture process (Melgar and Hayes, 2019; Colombelli et al., 2020). Similarly, prediction horizons comparable with a fraction of slip duration have been suggested for SSEs from Cascadia (Gualandi et al., 2020) and Hikurangi (shallow SSEs, Truttmann et al., 2024). Note though that algorithms exist that can forecast the evolution of a dynamical system multiple Lyapunov times ahead (e.g., Pathak et al., 2018). Ultimately, it is very likely that systems like Gelquakes, Foamquakes, slow and regular earthquakes are all characterized by different levels of predictability at different stages of the seismic cycle (or, to be more precise, in different portions of their phase space). Further studies, using recently developed tools to address exactly this problem (Dong, 2024), will be carried out in the future.

Previous estimations of seismotectonic models' predictability based on deep learning (DL) display prediction horizons similar to those obtained in this study (Mastella et al., 2022a), matching estimations based on the metric entropy. Recent studies support the capability of DL to extend even further entropy-based prediction horizons (e.g., Pathak et al., 2018) providing a source of optimism for future applications.

A further remark supporting the analogy of scaled seismotectonic models with SSEs concerns the framing of the experiments into the rate and state friction framework (e.g., Scholz, 1998), especially when focusing on the Dieterich-Ruina-Rice number (Ru ; Dieterich, 1979; Rice and Ruina, 1983). Ru is a parameter proportional to the ratio of the asperity size to the critical nucleation size. When changed, it modifies rupture behavior, recurrence time, and slip rates (e.g., Barbot, 2019). Interestingly, the combinations of rate and state parameters that allow the numerical modeling of Foamquake behavior is compatible with low Ru values (Corbi et al., 2024), similar to those that lead to slow earthquakes based on numerical simulations (Barbot, 2019).

The path of $d1$ and θ through the seismic cycle is dif-

ferent in our experiments and SSEs. In particular, SSEs are characterized by higher $d1$ at the onset and end of slip episodes (Gualandi et al., 2020), while in the lab we found higher $d1$ during slip episodes. This difference is likely due to the different observables chosen to describe system dynamics (i.e., displacement for our experiments and slip potency rate for SSEs). The high coseismic $d1$ values observed in our experiments mirror the focus of displacement trajectories during this stage (Figure S10). The choice of the observable to analyze can influence the retrieved nonlinear dynamical indices (e.g., Lorenz, 1991), and the differences between slip potency and slip potency rate have been preliminary investigated in the case of Cascadia SSEs (Gualandi et al., 2020). A systematic assessment of how the selected observable plays a role in determining system dynamics will be the subject of future studies. Additionally, for Gelquake we identified a clear decrease of θ that alerts the onset of slip (Figure 4B). This signal is likely absent for SSEs, and in the lab emerges only when focusing into asperity dynamics (Figure S6). This observation highlights the importance of precisely mapping interplate coupling, e.g. via seafloor geodetic constraints (Yokota et al., 2016) and paves the way for the next discussion point.

5.3 Relevance for the seismic cycle

Recent seismological and geodetic observations suggest that large earthquakes may be preceded by gradual fault failure as testified by foreshocks, decrease of interplate coupling, and/or precursory aseismic slip (Schurr et al., 2014; Mavrommatis et al., 2014; Bouchon et al., 2015; Kato and Ben-Zion, 2020). These phenomena depict the transition from a deceleration of seismic moment accumulation toward a sudden acceleration during an earthquake. In our experiments, both interseismic slowdown and slow frictional instability nucleation occur in the form of a relatively persistent state in the phase space, as highlighted by the decrease of θ . This signal might be interpreted optimistically as a precursor. However, our study emphasizes the challenge of generalizing. In fact, the late interseismic θ reduction a) requires precise asperity area monitoring; and b) is absent in Foamquake. The latter observation shows us the importance of the monitoring frequency with respect to the timescale of slip episodes. We expect that the analog fault of Foamquake unlocks rapidly, and the monitoring rate is not high enough to capture this process. It is indeed challenging to provide a comprehensive understanding of this timescale in nature. It has been argued that gradual fault unlocking and precursory slip may occur several hours (an average after stacking tens of events, e.g., Bletery and Nocquet, 2023) - months (e.g., Schurr et al., 2014) - years (Mavrommatis et al., 2014; Bouchon et al., 2015) before large earthquakes. Current monitoring systems can resolve such timescales, but the existence of a reliable precursor in seismic or geodetic data remains elusive (e.g., Bürgmann, 2023). We highlighted the similarity between predictability horizons of slip phases in the order of a fraction of slip duration for SSEs in nature and for laboratory earth-

quakes in our experiments. If a similar horizon in the order of a fraction of slip event duration is characteristic of frictional physics across scales, then for large subduction earthquakes we can expect predictability horizons smaller than hundreds of seconds. This timing is shorter than the hours-to-years geodetic and seismological indicators mentioned above, which suggests delving deeper into the topic.

Our results highlight the higher complexity of granular fault physics that complicates the seismic cycle behavior. In nature, other factors could likely impact fault behavior such as temperature, rheological and geometrical heterogeneities, effects of fluids, and stress interaction of adjacent fault systems. However, despite all those factors act in concert along subduction zones, it seems plausible to attempt setting up a reduced order model to describe the macroscopic behavior of stick-slip dynamics across scales. The next challenge is understanding whether similar conclusions hold also for large subduction earthquakes, ruling out whether their unpredictability is due to a) the complex nature of the Earth's crust (Main and Naylor, 2008; Bak, 1996; Rice, 1993); b) the temporally incomplete and spatially fragmentary observations (Main and Naylor, 2008); c) external perturbations (Gualandi et al., 2023; Matthews, 2002), or d) the fact that simple, deterministic systems can have unpredictable behavior (Huang and Turcotte, 1990; Becker, 2000), with previous points considered singularly or in ensemble.

Acknowledgements

The authors thank the reviewers, M. van den Ende and P. Bhattacharya, for their constructive comments. This research was supported by PRIN: Progetti di ricerca di rilevante interesse nazionale codice progetto 2022MJ82MC (PREVENT) and fondazione CARIPOLO for Supporto ai giovani talenti italiani nelle competizioni dell' European Research Council (2023-2518; SENTINEL) to F.C. F.F. thanks EPOS ITALIA and the Grant to Department of Science, Roma Tre University (MIUR-Italy Dipartimenti di Eccellenza, ARTICOLO 1, COMMI 314 – 337 LEGGE 232/2016).

Data and code availability

Surface velocity data from Foamquake models is available open access through the GFZ data repository reported in Mastella et al. (2021). Surface velocity data from Gelquake model in twin asperity configuration is available open access through the GFZ data repository reported in Corbi et al. (2021). For all experiments reported in this study, displacement time series sampled along the cross-section striking parallel to the seismogenic zone are accessible open access via Zenodo at the link <https://doi.org/10.5281/zenodo.13683309>, together with a Matlab file that allows reproducing Figures S1-S4.

To compute AMI, we used the Matlab function `phaseSpaceReconstruction`. Plots of $AMI(\tau)$ realized using the `ARFM_ami.m` function (Sujith, 2019). To compute $E1(m)$ and $E2(m)$ we

used the Matlab function `cao_deneme.m` by M. Kizilkaya. To compute $d1$ and θ we used the Matlab function `fun_dynsys_univariate_analysis.m` by D. Faranda. Both `cao_deneme.m` and `fun_dynsys_univariate_analysis.m` are available through the MathWorks File Exchange portal. The pseudo code to perform NFA can be found in Gualandi et al. (2020).

Competing interests

The authors declare no competing interests.

References

- Avouac, J.-P. From Geodetic Imaging of Seismic and Aseismic Fault Slip to Dynamic Modeling of the Seismic Cycle. *Annual Review of Earth and Planetary Sciences*, 43(1):233–271, May 2015. doi: 10.1146/annurev-earth-060614-105302.
- Bak, P. *The Discovery of Self-Organized Criticality*, page 33–48. Springer New York, 1996. doi: 10.1007/978-1-4757-5426-1_2.
- Barbot, S. Slow-slip, slow earthquakes, period-two cycles, full and partial ruptures, and deterministic chaos in a single asperity fault. *Tectonophysics*, 768:228171, Oct. 2019. doi: 10.1016/j.tecto.2019.228171.
- Becker, T. W. *Deterministic chaos in two state-variable friction sliders and the effect of elastic interactions*, page 5–26. American Geophysical Union, 2000. doi: 10.1029/gm120p0005.
- Bletery, Q. and Nocquet, J.-M. The precursory phase of large earthquakes. *Science*, 381(6655):297–301, July 2023. doi: 10.1126/science.adg2565.
- Boffetta, G., Cencini, M., Falcioni, M., and Vulpiani, A. Predictability: a way to characterize complexity. *Physics Reports*, 356(6): 367–474, Jan. 2002. doi: 10.1016/s0370-1573(01)00025-4.
- Bouchon, M., Durand, V., Marsan, D., Karabulut, H., and Schmitzbuhl, J. The long precursory phase of most large interplate earthquakes. *Nature Geoscience*, 8(2):83–83, Feb. 2015. doi: 10.1038/ngeo1770.
- Brizzi, S., van Zelst, I., Funicello, F., Corbi, F., and van Dinther, Y. How Sediment Thickness Influences Subduction Dynamics and Seismicity. *Journal of Geophysical Research: Solid Earth*, 125(8), July 2020. doi: 10.1029/2019jb018964.
- Bürgmann, R. Reliable earthquake precursors? *Science*, 381(6655):266–267, July 2023. doi: 10.1126/science.adi8032.
- Cao, L. Practical method for determining the minimum embedding dimension of a scalar time series. *Physica D: Nonlinear Phenomena*, 110(1–2):43–50, Dec. 1997. doi: 10.1016/s0167-2789(97)00118-8.
- Colombelli, S., Festa, G., and Zollo, A. Early rupture signals predict the final earthquake size. *Geophysical Journal International*, 223(1):692–706, July 2020. doi: 10.1093/gji/ggaa343.
- Corbi, F., Funicello, F., Moroni, M., van Dinther, Y., Mai, P. M., Dalguer, L. A., and Faccenna, C. The seismic cycle at subduction thrusts: 1. Insights from laboratory models. *Journal of Geophysical Research: Solid Earth*, 118(4):1483–1501, Apr. 2013. doi: 10.1029/2012jb009481.
- Corbi, F., Funicello, F., Brizzi, S., Lallemand, S., and Rosenau, M. Control of asperities size and spacing on seismic behavior of subduction megathrusts. *Geophysical Research Letters*, 44(16): 8227–8235, Aug. 2017. doi: 10.1002/2017gl074182.
- Corbi, F., Sandri, L., Bedford, J., Funicello, F., Brizzi, S., Rosenau, M., and Lallemand, S. Machine Learning Can Predict the Timing

- and Size of Analog Earthquakes. *Geophysical Research Letters*, 46(3):1303–1311, Feb. 2019. doi: 10.1029/2018gl081251.
- Corbi, F., Bedford, J., Poli, P., Funicello, F., and Deng, Z. Particle image velocimetry data from an analog seismo-tectonic model addressing the interaction between neighbor asperities, 2021. doi: 10.5880/FIDGEO.2021.038.
- Corbi, F., Mastella, G., Tinti, E., Rosenau, M., Sandri, L., Pardo, S., and Funicello, F. Asperity Size and Neighboring Segments Can Change the Frictional Response and Fault Slip Behavior: Insights From Laboratory Experiments and Numerical Simulations. *Journal of Geophysical Research: Solid Earth*, 129(1), Jan. 2024. doi: 10.1029/2023jb026594.
- Datseris, G., Kottlarz, I., Braun, A. P., and Parlitz, U. Estimating fractal dimensions: A comparative review and open source implementations. *Chaos: An Interdisciplinary Journal of Nonlinear Science*, 33(10), Oct. 2023. doi: 10.1063/5.0160394.
- Dieterich, J. H. Modeling of rock friction: 1. Experimental results and constitutive equations. *Journal of Geophysical Research: Solid Earth*, 84(B5):2161–2168, May 1979. doi: 10.1029/jb084ib05p02161.
- Dong. Revisiting the predictability of dynamical systems: a new local data-driven approach. *ArXiv*, 2024. doi: 10.48550/arXiv.2409.14865.
- Eckmann, J.-P. and Ruelle, D. *Ergodic theory of chaos and strange attractors*, page 273–312. Springer New York, 1985. doi: 10.1007/978-0-387-21830-4_17.
- Faranda, D. and Vaienti, S. Correlation dimension and phase space contraction via extreme value theory. *Chaos: An Interdisciplinary Journal of Nonlinear Science*, 28(4), Apr. 2018. doi: 10.1063/1.5027386.
- Faranda, D., Messori, G., and Yiou, P. Dynamical proxies of North Atlantic predictability and extremes. *Scientific Reports*, 7(1), Jan. 2017. doi: 10.1038/srep41278.
- Farmer, J. D. and Sidorowich, J. J. Predicting chaotic time series. *Physical Review Letters*, 59(8):845–848, Aug. 1987. doi: 10.1103/physrevlett.59.845.
- Fraser, A. M. and Swinney, H. L. Independent coordinates for strange attractors from mutual information. *Physical Review A*, 33(2):1134–1140, Feb. 1986. doi: 10.1103/physreva.33.1134.
- Funicello, F. and Corbi, F. *Analog Models for Earth Sciences*, page 856–867. Elsevier, 2021. doi: 10.1016/b978-0-08-102908-4.00078-3.
- Gualandi, A., Avouac, J.-P., Michel, S., and Faranda, D. The predictable chaos of slow earthquakes. *Science Advances*, 6(27), July 2020. doi: 10.1126/sciadv.aaz5548.
- Gualandi, A., Faranda, D., Marone, C., Cocco, M., and Mengaldo, G. Deterministic and stochastic chaos characterize laboratory earthquakes. *Earth and Planetary Science Letters*, 604:117995, Feb. 2023. doi: 10.1016/j.epsl.2023.117995.
- Gualandi, A., Dal Zilio, L., Faranda, D., and Mengaldo, G. Similarities and Differences Between Natural and Simulated Slow Earthquakes. *Geophysical Research Letters*, 51(14), July 2024. doi: 10.1029/2024gl109845.
- Heuret, A., Lallemand, S., Funicello, F., Piromallo, C., and Facenna, C. Physical characteristics of subduction interface type seismogenic zones revisited. *Geochemistry, Geophysics, Geosystems*, 12(1), Jan. 2011. doi: 10.1029/2010gc003230.
- Huang, J. and Turcotte, D. L. Are earthquakes an example of deterministic chaos? *Geophysical Research Letters*, 17(3):223–226, Mar. 1990. doi: 10.1029/gl017i003p00223.
- Hubbert, M. K. Theory of scale models as applied to the study of geologic structures. *Geological Society of America Bulletin*, 48(10):1459–1520, Oct. 1937. doi: 10.1130/gsab-48-1459.
- Huke, J. *Embedding Nonlinear Dynamical Systems: A Guide to Takens' Theorem*, 2006.
- Kato, A. and Ben-Zion, Y. The generation of large earthquakes. *Nature Reviews Earth and Environment*, 2(1):26–39, Nov. 2020. doi: 10.1038/s43017-020-00108-w.
- Lorenz, E. N. Dimension of weather and climate attractors. *Nature*, 353(6341):241–244, Sept. 1991. doi: 10.1038/353241a0.
- Main, I. G. and Naylor, M. Maximum entropy production and earthquake dynamics. *Geophysical Research Letters*, 35(19), Oct. 2008. doi: 10.1029/2008gl035590.
- Mastella, G., Corbi, F., Funicello, F., and Matthias, R. Particle image correlation data from Foamquake: a novel seismotectonic analog model mimicking the megathrust seismic cycle, 2021. doi: 10.5880/FIDGEO.2021.046.
- Mastella, G., Corbi, F., Bedford, J., Funicello, F., and Rosenau, M. Forecasting Surface Velocity Fields Associated With Laboratory Seismic Cycles Using Deep Learning. *Geophysical Research Letters*, 49(15), Aug. 2022a. doi: 10.1029/2022gl099632.
- Mastella, G., Corbi, F., Funicello, F., and Rosenau, M. Foamquake: A Novel Analog Model Mimicking Megathrust Seismic Cycles. *Journal of Geophysical Research: Solid Earth*, 127(3), Feb. 2022b. doi: 10.1029/2021jb022789.
- Matthews, M. V. A Brownian Model for Recurrent Earthquakes. *Bulletin of the Seismological Society of America*, 92(6):2233–2250, Aug. 2002. doi: 10.1785/0120010267.
- Mavrommatis, A., Segall, P., and Johnson, K. A decadal-scale deformation transient prior to the 2011 Mw 9.0 Tohoku-oki earthquake. *Geophysical Research Letters*, 41(8):2671–2672, Apr. 2014. doi: 10.1002/2014GL060139.
- Meier, M.-A., Ampuero, J. P., and Heaton, T. H. The hidden simplicity of subduction megathrust earthquakes. *Science*, 357(6357):1277–1281, Sept. 2017. doi: 10.1126/science.aan5643.
- Melgar, D. and Hayes, G. P. Characterizing large earthquakes before rupture is complete. *Science Advances*, 5(5), May 2019. doi: 10.1126/sciadv.aav2032.
- Michel, S., Gualandi, A., and Avouac, J.-P. Interseismic Coupling and Slow Slip Events on the Cascadia Megathrust. *Pure and Applied Geophysics*, 176(9):3867–3891, Sept. 2018. doi: 10.1007/s00024-018-1991-x.
- Moreno, M., Rosenau, M., and Oncken, O. 2010 Maule earthquake slip correlates with pre-seismic locking of Andean subduction zone. *Nature*, 467(7312):198–202, Sept. 2010. doi: 10.1038/nature09349.
- Pathak, J., Hunt, B., Girvan, M., Lu, Z., and Ott, E. Model-Free Prediction of Large Spatiotemporally Chaotic Systems from Data: A Reservoir Computing Approach. *Physical Review Letters*, 120(2), Jan. 2018. doi: 10.1103/physrevlett.120.024102.
- Pluijm, B. and Marshak, S. *Earth Structure: An Introduction*. W. W. Norton Company, 2004.
- Rice, J. R. Spatio-temporal complexity of slip on a fault. *Journal of Geophysical Research: Solid Earth*, 98(B6):9885–9907, 1993. doi: https://doi.org/10.1029/93JB00191.
- Rice, J. R. and Ruina, A. L. Stability of Steady Frictional Slipping. *Journal of Applied Mechanics*, 50(2):343–349, June 1983. doi: 10.1115/1.3167042.
- Rosenau, M., Horenko, I., Corbi, F., Rudolf, M., Kornhuber, R., and Oncken, O. Synchronization of Great Subduction Megathrust Earthquakes: Insights From Scale Model Analysis. *Journal of Geophysical Research: Solid Earth*, 124(4):3646–3661, 2019. doi: https://doi.org/10.1029/2018JB016597.
- Sauer, T., Yorke, J. A., and Casdagli, M. Embedology. *Journal of Statistical Physics*, 65(3–4):579–616, Nov. 1991. doi: 10.1007/BF01010101.

10.1007/bf01053745.

Scholz, C. H. Earthquakes and friction laws. *Nature*, 391(6662): 37–42, Jan. 1998. doi: 10.1038/34097.

Schurr, B., Asch, G., Hainzl, S., Bedford, J., Hoechner, A., Palo, M., Wang, R., Moreno, M., Bartsch, M., Zhang, Y., Oncken, O., Tilmann, F., Dahm, T., Victor, P., Barrientos, S., and Vilotte, J.-P. Gradual unlocking of plate boundary controlled initiation of the 2014 Iquique earthquake. *Nature*, 512(7514):299–302, Aug. 2014. doi: 10.1038/nature13681.

Scuderi, M. M., Marone, C., Tinti, E., Di Stefano, G., and Collettini, C. Precursory changes in seismic velocity for the spectrum of earthquake failure modes. *Nature Geoscience*, 9(9):695–700, Aug. 2016. doi: 10.1038/ngeo2775.

Strogatz, S. H. *Nonlinear Dynamics and Chaos: With Applications to Physics, Biology, Chemistry, and Engineering*. Chapman and Hall/CRC, Jan. 2024. doi: 10.1201/9780429398490.

Sveen, J. An introduction to matpiv v.1.6.1 Eprint, 2004. <http://urn.nb.no/URN:NBN:no-27806>. Retrieved from.

Takens, F. *Detecting strange attractors in turbulence*, page 366–381. Springer Berlin Heidelberg, 1981. doi: 10.1007/bfb0091924.

Theiler, J. Estimating fractal dimension. *Journal of the Optical Society of America A*, 7(6):1055, June 1990. doi: 10.1364/josaa.7.001055.

Truttmann, S., Poulet, T., Wallace, L., Herwegh, M., and Veveakis, M. Slow Slip Events in New Zealand: Irregular, yet Predictable? *Geophysical Research Letters*, 51(6), Mar. 2024. doi: 10.1029/2023gl107741.

Wales, D. J. Calculating the rate of loss of information from chaotic time series by forecasting. *Nature*, 350(6318):485–488, Apr. 1991. doi: 10.1038/350485a0.

Xia, K., Rosakis, A. J., and Kanamori, H. Laboratory Earthquakes: The Sub-Rayleigh-to-Supershear Rupture Transition. *Science*, 303(5665):1859–1861, Mar. 2004. doi: 10.1126/science.1094022.

Yokota, Y., Ishikawa, T., Watanabe, S.-i., Tashiro, T., and Asada, A. Seafloor geodetic constraints on interplate coupling of the Nankai Trough megathrust zone. *Nature*, 534(7607):374–377, May 2016. doi: 10.1038/nature17632.

The article *Scaled seismotectonic models of megathrust seismic cycles through the lens of dynamical systems theory* © 2025 by F. Corbi is licensed under CC BY 4.0.